Materials Science Forum
ISSN: 1662-9752, Vol. 1175, pp 105-110
doi:10.4028/p-OOnKo3

Submitted: 2025-07-02
Revised: 2025-09-18
Accepted: 2025-10-21
Online: 2026-01-16

In situ Alloyed Refractory High Entropy Alloy by Laser Powder Bed Fusion

Yong Seong Kim[1,a], Ozkan Gokcekaya[1,2,b*], Ryosuke Ozasa[1,2,c] and Takayoshi Nakano[1,2,d*]

[1]Division of Materials and Manufacturing Science, Graduate School of Engineering, Osaka University, 2-1, Yamadaoka, Suita, Osaka 565-0871, Japan

[2]Anisotropic Design and Additive Manufacturing Research Center, Osaka University, 2-1, Yamadaoka, Suita, Osaka 565-0871, Japan

[a]yongseong.kim@mat.eng.osaka-u.ac.jp, [b]ozkan@mat.eng.osaka-u.ac.jp, [c]ozasa@mat.eng.osaka-u.ac.jp, [d]nakano@mat.eng.osaka-u.ac.jp

Keywords: High entropy alloys, Additive manufacturing, In-situ alloying, Segregation.

Abstract. Pre-alloyed powders, which are mainly used in laser powder bed fusion (LPBF), have the disadvantage of being time-consuming and costly to manufacture. To overcome these disadvantages, in-situ alloying, which mixes pure element powders and performs alloying in real time during the LPBF process, has been attracting attention. In particular, it is quite challenging to manufacture high entropy alloy (HEA) containing high melting point refractory elements by in-situ alloying. In this study, we designed a single-phase BCC refractory HEA with a mix of Ti, Nb, Mo, Ta, and W through thermodynamic calculations and fabricated the designed composition by LPBF by mixing powders of each element and performing in-situ alloying. High energy density and remelting effectively suppressed segregation of constituent elements, which caused a decrease in residual stress and increased relative density. Our study represents a pioneering attempt to manufacture in-situ alloyed HEA by LPBF and demonstrates the effectiveness of in-situ alloying using mixed powders.

Introduction

Laser powder bed fusion (LPBF) is attracting attention as a next-generation manufacturing method because it can suppress segregation of constituent elements at very high cooling rates as well as shape customization [1]. In general, pre-alloyed powders by gas atomization are used for LPBF, but there is a disadvantage that the time and cost required for production increase. In-situ alloying, which alloys in real time during the LPBF process, is attracting attention to overcome this fatal drawback. Since in-situ alloying uses mixed powders, it does not require the production of pre-alloyed powders, which saves time and costs. In the case of high entropy alloy (HEA), which has recently been spotlighted as a next-generation alloy due to its excellent mechanical properties and corrosion resistance, it is composed of five or more main elements, so it has a high degree of design freedom compared to existing alloys, and if it is manufactured through in-situ alloying using mixed powder, it is possible to manufacture it flexibly without limiting the degree of design freedom with accompanying time and cost efficiency.

Despite the synergy between in-situ alloying and HEA, research utilizing in-situ alloying in HEA is extremely limited, and most of the research is very passive in that only one type of powder is added to the pre-alloyed powder to modify composition rather than alloying. Important to note that segregation of constituent elements and defects/cracks are inevitable due to the unique super-multicomponent nature of HEA and the high cooling rate of LPBF. In order to maximize the unique characteristics of HEA, such as solid solution strengthening, it is necessary to suppress segregation of constituent elements and prevent defect formation.

Therefore, this study discusses the correlation between segregation and crack mechanisms of in-situ alloyed HEAs by LPBF using mixed powders, a topic for which limited research has been conducted to date. Furthermore, the effect of segregation on densification and mechanical properties is discussed.

Experimental Procedures

For the optimization of alloy design, thermodynamic parameters were calculated, such as mixing entropy ($\Delta S_{mix}/R$), mixing enthalpy (ΔH_{mix}), atomic radius mismatch (δ), valence electron concentration (VEC), electronegativity ($\Delta\chi_{Allen}$), melting point mismatch (ΔT_m), and difference between liquidus and solidus temperature (ΔT) [2].

Based on the optimized composition, Ti, Nb, Mo, Ta, and W powders were mixed using a rocking mixer, and the process was conducted for 12 hours for uniformity. The mixed powders were manufactured into a size of 5 mm × 5 mm × 5 mm by an LPBF machine (EOS M290, EOS, Germany). The scanning strategy was applied as a Single XY-scan, in which the scanning direction rotates 90° for each layer, and a Double XY-scan, in which the scanning direction is rotated 90° after each layer and before applying the powder bed. The laser power (P) and scan speed (v) were in the range of 180-300 W and 400-800 mm/s, respectively, and a consistent hatch space (d) of 0.08 mm and layer thickness (t) of 0.02 mm were applied. The volume energy density (VED) was calculated by the following equation (1):

$$VED = P/vtd \ [J/mm^3]. \quad (1)$$

The relative density (relative density% = 100% − crack density%) of the samples fabricated through LPBF was calculated using an optical microscope and ImageJ software. The microstructure was investigated using a field-emission scanning electron microscope (FE-SEM; JIB-4610F, JEOL, Japan) equipped with an energy-dispersive X-ray spectrometer (EDS; X-MaxN, Oxford Instruments, UK). Nano-hardness was measured using a nano-indentation tester (ENT-1100, Elionix Corp., Japan) at a test load of 15 mN (P_{max}) with a continuous load rate of 1 mN/s for 100 seconds at P_{max}.

Results

Fig. 1 shows the alloy design using thermodynamic calculations and CALPHAD. For the design of biocompatible HEA, we selected Ti, Nb, Mo, Ta, and W, which have the smallest atomic radius difference among the elements that do not exhibit cytotoxicity. Then, as shown in Fig. 1(a), we first considered the composition (in red box) that satisfies the conditions for forming a solid solution, such as the mixing enthalpy ($-5 < \Delta H_{mix} < 5$) and the range of the melting point difference ($\Delta T_m < 16$) [2]. Fig. 1(b) shows the composition with a $\Delta S_{mix}/R \geq 1.5$ inside the red box in Fig. 1(a), and it is plotted against VEC, electronegativity, and ΔT. We finally selected $Ti_1(NbMoTa)_2W_{0.5}$, which satisfies the smallest VEC, electronegativity, and ΔT simultaneously. The thermodynamic parameters of the optimized alloy are shown in Table 1.

Table 1 Thermodynamic parameters of the $Ti_1(NbMoTa)_2W_{0.5}$ HEA.

	$\Delta S_{mix}/R$	ΔH_{mix} [kJ/mol]	δ [%]	VEC	$\Delta\chi_{Allen}$ [%]	ΔT_m [%]	ΔT [K]
$Ti_1(NbMoTa)_2W_{0.5}$	1.51	-4.6	2.53	5.2	3.6	15.7	22.2

Fig. 2(a) shows the SEM-EDS image of the mixed powder. The mixing was done for 12 hours using a rocking mixer, and the high uniformity of the mixed powder can be confirmed. Fig. 2(b) shows a schematic image of real-time alloying during the LPBF process using the mixed powder.

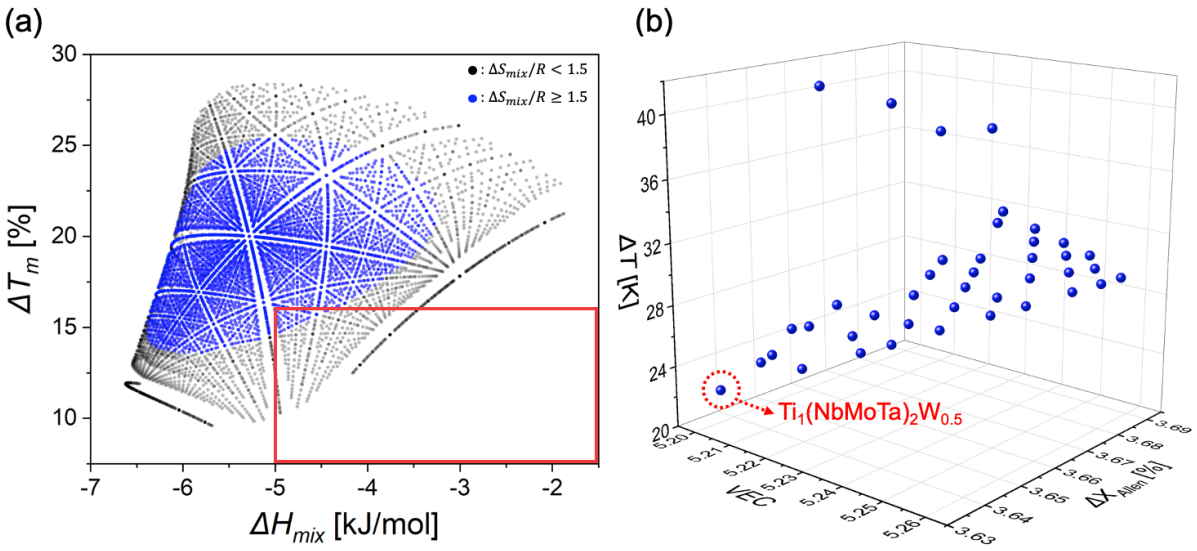

Fig. 1 Thermodynamic parameters calculation to predict solid solution formation of HEAs.(a) Relationship between the melting point mismatch (ΔT_m) and mixing enthalpy (ΔH_{mix}) (b) Relationship between the liquidus – solidus temperature (ΔT), valance electron concentration (VEC) and electronegativity ($\Delta\chi_{Allen}$) which satisfy $-5 < \Delta H_{mix} < 5$, $\Delta T_m < 16$ at the same time (red rectangle in (a)).

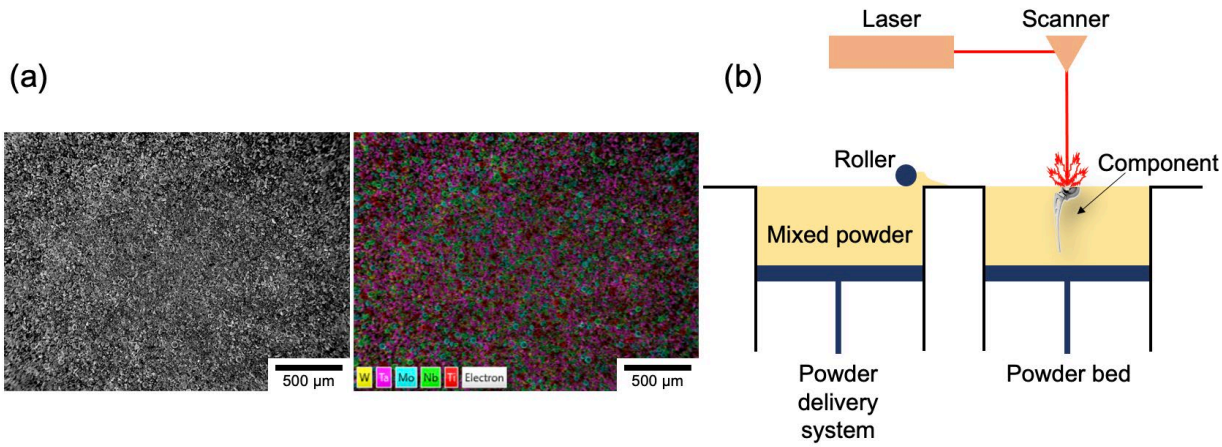

Fig. 2 (a) SEM-EDS of mixed powder (b) Schematic representation of laser powder bed fusion system.

Fig. 3 shows the optical microscope (OM) image and relative density observed in the yz-plane, and the scan strategies are Single XY-scan and Double XY-scan. In the case of low VED, the irregularity of cracks was observed, but as the VED increased, the transverse cracks were suppressed and aligned in the building direction (BD, z-axis). The trend of VED and relative density can be confirmed in Fig. 4, and it showed a proportional relationship regardless of the scan strategy. In addition, when the Double XY-scan was applied, the highest relative density of 98.1% was shown due to the effect of high VED and remelting. We selected three samples to analyze the effects of VED and remelting in more detail and named them S100 (VED: 150 J/mm^3), S300 (VED: 375 J/mm^3), and D300 (VED: 375 J/mm^3), respectively. Here, S and D stand for Single XY-scan and Double XY-scan, respectively, and the number following them indicates VED.

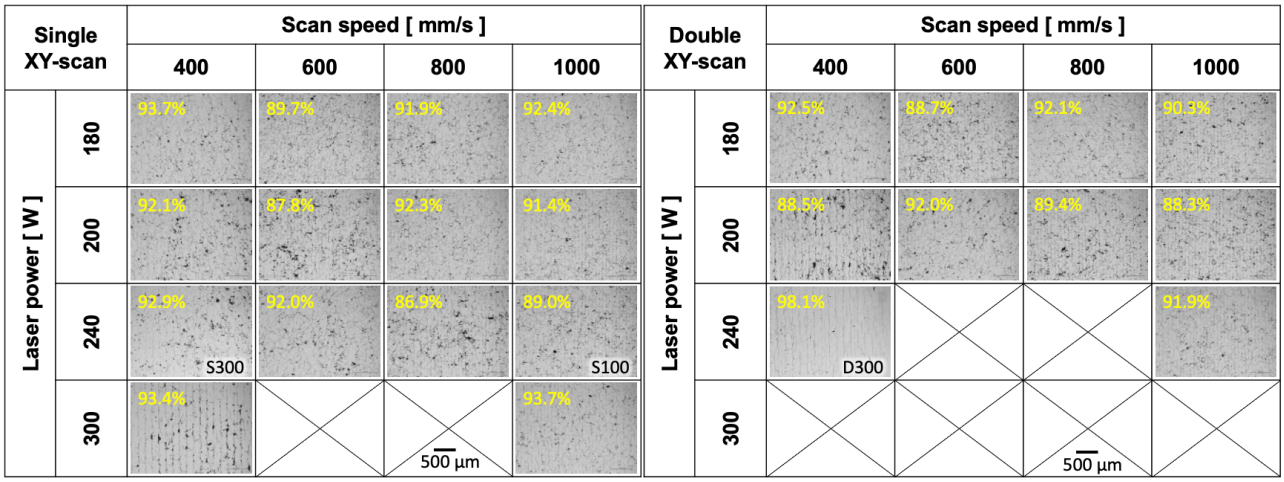

Fig. 3 OM images $Ti_1(NbMoTa)_2W_{0.5}$ by LPBF with various process parameter in Single and Double XY-scan strategy observed at yz-plane.

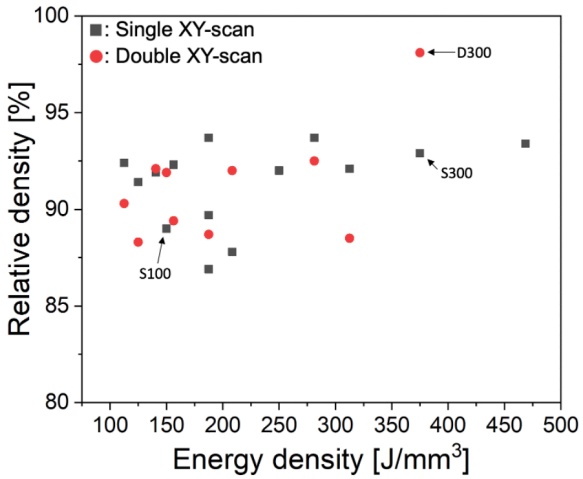

Fig. 4 Effect of energy density on relative density by image analysis in OM images with Single and Double XY-scan strategy.

Discussion

Effect of VED and remelting on microstructure. Fig. 5 (a-c) shows the backscattered electron (BSE) image and the corresponding EDS mapping image taken by SEM. In the S100 sample, unmelted powder and elements that were melted but not completely dissolved were confirmed. This is thought to be due to insufficient Marangoni force due to low VED. In addition, cracks were confirmed to have occurred around the elements that were not completely dissolved, and it can be seen that these are the transverse cracks observed in the OM images of Fig. 3. Some areas where non-uniform melting was not achieved caused the presence of liquid metal. The shrinkage due to solidification of the liquid metal induces high residual stress, and the residual stress acts as the initiation point of the crack [3]. In the S300, a relatively uniform element distribution was observed due to the increased VED, but segregation was observed in some areas. In D300 with additional remelting applied, unmelted powder was not observed, and a uniform element distribution was achieved. Fig. 5(d) shows the actual composition obtained through EDS mapping, divided by the design composition, to quantitatively represent segregation. The closer this value is to 1, the more suppressed segregation is, and the closer the composition is to the design composition. This demonstrates that an increase in VED (S300) and remelting (D300) are effective in suppressing segregation. Suppression of segregation led to suppression of residual stress, unlike low VED, and as a result, transverse cracks were suppressed, and cracks mainly aligned in the BD direction at the center of the melt pool could be observed. Suppression of transverse cracks resulted in a decrease in crack density and an increase in relative density. The high density led to a significant improvement in mechanical properties. Fig. 6 shows the results of nano-indentation, and the increase in relative

density due to crack suppression contributed to the improvement of the material's mechanical properties. Table 2 summarizes the correlations among VED, crack density, relative density, and nanohardness described above. Increased VED and the application of remelting suppress segregation of constituent elements, which in turn affects crack density, relative density, and mechanical properties.

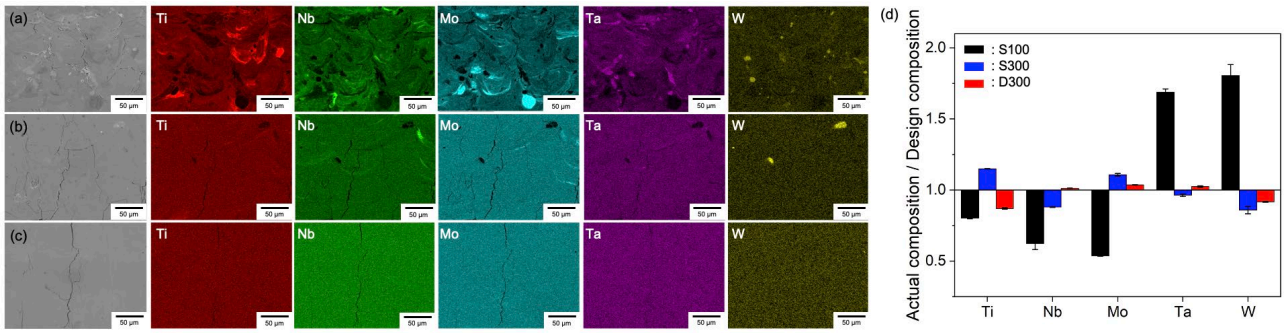

Fig. 5 SEM-EDS images of (a) S100, (b) S300, and (c) D300, including elemental mapping of Ti, Nb, Mo, Ta, and W. And the corresponding EDS qualitative mapping analysis.

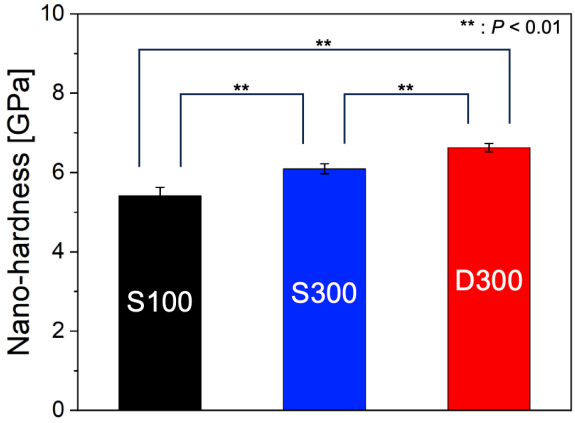

Fig. 6 Nano-hardness of in-situ alloyed HEA. ** : $P < 0.01$ by Tukey's test.

Table 2 Correlation between VED, Crack density, Relative density, and Nano-hardness

	VED [J/mm^3]	Crack density [%]	Relative density [%]	Nano-hardness [GPa]
S100	150	11.0	89.0	5.42 ± 0.2
S300	375	7.1	92.9	6.10 ± 0.1
D300	375x2	1.9	98.1	6.63 ± 0.1

Crack mechanism in in-situ alloying. Fig. 7 shows the crack formation mechanism based on the analysis so far. In the low VED represented by sample S100, there were many unmelted powders due to insufficient energy density. During rapid solidification, elemental segregation induced residual stress, which acted as the initiation point of cracks, and the cracks propagated along the segregated regions and grain boundaries. As a result, a disorderly crack distribution was observed. In sample S300, represented by high VED, a deeper melt pool was formed due to the increased VED, and a mostly uniform element distribution was observed due to the increased Marangoni force, but unmelted powders were still observed in some areas. However, in D300, where remelting was applied, a wider melt pool was formed owing to the heat accumulation from the melting of the previous layer, which promoted the homogenization of the microstructure, eliminating unmelted powders and segregated elements. As a result, the suppressed segregation reduced the residual stress [3], and the highest relative density was observed. Also, unlike other samples, D300 showed cracks

aligned in the BD direction along high-angle grain boundaries (HAGBs), while the transverse cracks were suppressed. This is due to the difference in the temperature gradient direction between the melt pool side and the melt pool center. At the melt pool side, the temperature gradient is formed in the vertical direction of the melt pool (45 degrees to BD), and at the melt pool center, the temperature gradient is formed parallel to BD [4]. This difference in the temperature gradient direction forms HAGBs vulnerable to cracks at the center of the melt pool during solidification, where high stress accumulates, and thus the cracks propagate along the center of the melt pool [5].

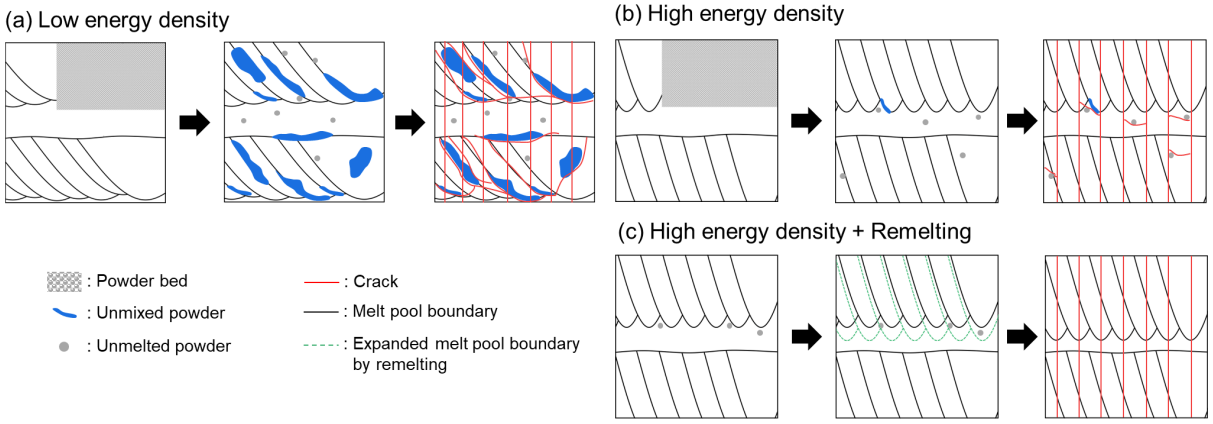

Fig. 7 Schematic representation of the crack mechanism in various process parameter conditions.

Summary

In this study, thermodynamic calculations were utilized to design an alloy that minimizes the difference between the liquidus and solidus lines to suppress segregation of HEA. In addition, to minimize the disadvantages of pre-alloyed powder, in-situ alloying was applied to manufacture HEA by mixing pure element powders and performing real-time alloying during the LPBF process. In D300, where high VED and remelting were applied simultaneously, it was confirmed that segregation was suppressed without unmelted powder. This induced an increase in relative density and mechanical properties due to a decrease in residual stress. Therefore, in-situ alloying, which performs real-time alloying during the LPBF process using mixed powders, can save time and cost, and the optimization of process parameters using remelting enabled the production of high-density samples.

References

[1] T. Ishimoto, R. Ozasa, K. Nakano, M. Weinmann, C. Schnitter, M. Stenzel, A. Matsugaki, T. Nagase, T. Matsuzaka, M. Todai, H.S. Kim, T. Nakano, Development of TiNbTaZrMo bio-high entropy alloy (BioHEA) super-solid solution by selective laser melting, and its improved mechanical property and biocompatibility, Scr. Mater. 194 (2021) 113658.

[2] Y.S. Kim, R. Ozasa, K. Sato, O. Gokcekaya, T. Nakano, Design and development of a novel non-equiatomic Ti-Nb-Mo-Ta-W refractory high entropy alloy with a single-phase body-centered cubic structure, Scr. Mater. 252 (2024) 116260.

[3] Y.S. Kim, O. Gokcekaya, A. Matsugaki, R. Ozasa, T. Nakano, Laser energy-dependent processability of non-equiatomic TiNbMoTaW high-entropy alloy through in-situ alloying of elemental feedstock powders by laser powder bed fusion, Materialia 38 (2024) 102241.

[4] T. Ishimoto, N. Morita, R. Ozasa, A. Matsugaki, O. Gokcekaya, S. Higashino, M. Tane, T. Mayama, K. Cho, H.Y. Yasuda, Superimpositional design of crystallographic textures and macroscopic shapes via metal additive manufacturing—Game-change in component design, Acta Mater. 286 (2025) 120709.

[5] Y.S. Kim, O. Gokcekaya, K. Sato, R. Ozasa, A. Matsugaki, T. Nakano, In-situ alloying of nonequiatomic TiNbMoTaW refractory bio-high entropy alloy via laser powder bed fusion: Achieving suppressed microsegregation and texture formation, Mater. Des. 252 (2025) 113824.